Adjoint Based Multi-Objective Optimization of Submerged Subsonic Intake

Conference Paper · January 2021

DOI: 10.1109/IBCAST51254.2021.9393016

2 authors:

Ali Ahmed
Middle East Technical University
9 PUBLICATIONS **4** CITATIONS
SEE PROFILE

Ismail H. Tuncer
Middle East Technical University
119 PUBLICATIONS **1,271** CITATIONS
SEE PROFILE

ADJOINT BASED MULTI-OBJECTIVE OPTIMIZATION OF SUBMERGED SUBSONIC INTAKE

Ali Ahmed[1] and Ismail H. Tuncer[2]
Department of Aerospace Engineering
Middle East Technical University
06800 Ankara, TURKEY
e-mail[1]: ali.ahmed_01@metu.edu.tr email[2]: ismail.h.tuncer@ae.metu.edu.tr

2021 International Bhurban Conference on Applied Sciences and Technologies (IBCAST) | 978-1-6654-0516-4/21/$31.00 ©2021 IEEE | DOI: 10.1109/IBCAST51254.2021.9393016

***Abstract*— The present study describes the adjoint based shape optimization of sub-merged trapezoidal intake. Initially direct results on the baseline geometries are compared with published results which are found to be in good agreement. Thereafter study proceeds to shape optimization using as multi-objective optimization technique. The combined multi-objective objective function is employed, comprising of total pressure at AIP and lift of the aerodynamic body . The inherent shape of the sub-merged intake gives low drag but also low-pressure recovery, therefore lift as an additional objective can give advantage over other intake types. The study is performed using SU^2 the flow solver together with the built-in adjoint solver and the FFD box which is the shape deformation tool in a parallel computing environment. A reduction in total pressure loss of 10% was achieved at AIP while CL/CD increased for the overall body.**

Keywords—Submerged intake; Adjoint optimization; SU^2

I. INTRODUCTION

Intakes are integral part of air-breathing propulsion systems primarily for the provision of air to engines. In most aerodynamic vehicles with jet engines, the intakes are overwhelmingly pitot type subsonic intake.

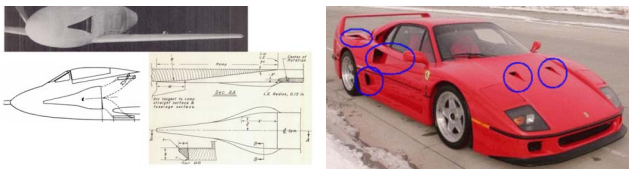

Figure 1: Examples of NACA type air intake
Left: YF-93 aircraft [1]. Right: Ferrari F40

However when jet engines were being developed during the 1940s, the submerged type was a major candidate as well for primary air supply however due to minor issues such as pressure recovery at transonic conditions the pitot type was given preference and submerged intake more or less was ignored [1]. Later, these types of intakes were used in auxiliary applications. Since, the absence of ram pressure adds to the challenge of improved performance other parameters are needed to be explored for trade-off. In this study an investigation into different objective functions as design parameters is done considering the special flow characteristic of these intakes. Submerged intakes, unlike pitot-type are non-protruding and can also be called flush intake as the duct of intake is flushed with the surface of the aerodynamic vehicle. Therefore, they are inherently devoid of creating any form drag which is a major advantage [2]. The duct usually rotates the flow coming in from a free stream to the engine face or the AIP. The flow would experience separation at the edges as well as at the bends in duct. Intuitively the quality of flow is disturbed with respect to total pressure losses along the duct and distortion therefore, any geometric detail which governs the flow quality are important. Several studies were carried out to improve air quality at the intake AIP using vortex generators [3] .The lip or intake edge is usually the part of intake where the intake flushes with the vehicle surface. The design of the lip or intake edge has been carried out previously by many studies which showing counter-rotating vortex-pairs emanating at the sharp corners in case of NACA type intake as well as trapezoidal intake. This vortex pair entrain the flow into the intake duct as well as they may contribute to negative Cp distribution on the ramp surface upstream of the duct. The strength and shape of this vortex pair depend upon the side edge geometry and the back-pressure conditions. The possibility of extracting lift because of negative Cp distribution and hence the low drag are attractive features of submerged intake and can be considered as key trade-off parameters against conventional pitot type subsonic intakes.

The shape optimization methods recently developed using adjoint techniques are a game changer in field of aerodynamics. The use of adjoint for shape optimization is a fairly recent endeavor. Jameson introduced the use of adjoint

1 Phd Student Aerospace Engineering Deptt. METU
2 Prof. Dr. and Chairman Aerospace Engineering Deptt. METU

978-0-7381-0535-2/21/$31.00 ©2021 IEEE

based and derived equations coupling gradient of optimization and Navier-Stokes equation [4]. Brezilion and Gauger optimized 2D airfoils and 3D wings using adjoint method [5]. Adjoint methods employ gradient calculation to find the optimum which may end up being the local optimum of the objective function unlike Genetic Algorithms GA which are basically employed to find the global optimum. A widely cited study is done by Taskinoglu who employed GA based technique to optimize a submerged intake [6].

In the present study, the open source SU^2 flow solver together with the built-in adjoint based aerodynamic shape optimization and solution adapted grid refinement tools is used to optimize the submerged intake configuration . The baseline configuration used in the present study is obtained from a published work on trapezoidal intake on slender body by Shu Sun et al [7] which comprise both numerical and experimental results.In this study an effort is done to implement end-to-end openware tools from CAD modeling to shape optimization. The compatibility of using different platform is a major issue which is also resolved by using the process cycle as shown in figure 3. The geometric modeling is done on SALOME CAD software while the hybrid mesh for 3D RANS solution is generated using GMSH.

Initially flow solved on SU2 direct solver is compared and verified from reference study. SU2 has the capability to solve fluid flow using RANS and it is fully integrated with the shape optimzation tools [8]. The baseline mesh with reference geometry is contained in a FFD box mesh and finally optimization cycles commence. In each step of the design optimization cycle the shape is deformed by a certain measure and sensitivity or adjoint of the objective function is obtained for the deformation. Finally, a direct CFD run gives the flow solution and value of updated objective function. The flow is visualized in PARAVIEW post processing package.

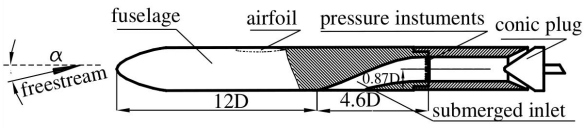

Figure 2: Reference Geometry for a trapezoidal flush intake [2].

II. METHODOLOGY

The general methodology of any CFD based optimization consists of two parts: basic flow study which consists of geometric and mesh modelling and solving Reynolds averaged Navier-Stokes equations which gives the baseline flow solution and corresponding values of the objective function. This baseline geometry and solution is thereafter optimized using design cycles in which deformation, adjoint calculation and direct solver is used iteratively till optimized design is achieved. In the present study the same methodology is followed in terms of the tools used in each step as shown in figure 3. Some details of these tools are given as follows:

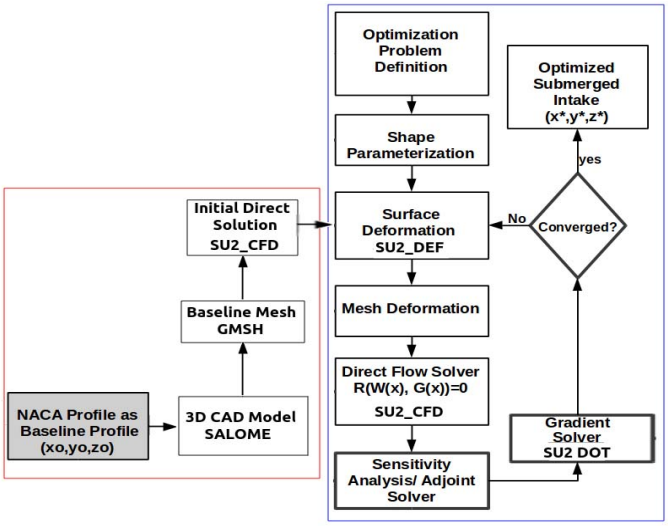

Figure 3: SU2 based CFD and adjoint optimization flow chart.

A. *Geometry and Mesh Generation*

The geometry for the present study is obtained from a published study in which characterization of the submerged intake is done by varying side edge and ramp angle at operating Mach no of 0.73 based on both experimental and numerical results [7]. The reference trapezoidal intake geometry and placement in the slender body is shown in figure 2. The same geometry was modeled in SALOME for 4° side edge angle and 23° ramp angle. The modeled geometry was flipped over such that the intake faced towards the positive y-direction. This was done in order to align the geometry for lift optimization as shown in figure 4.

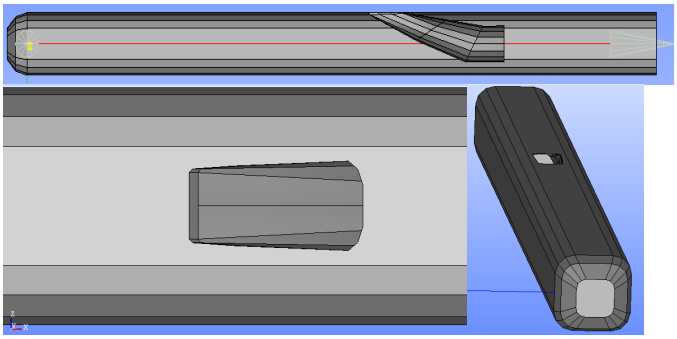

Figure 4: SALOME modeled slender Body with Intake

GMSH [9] is used to generate hybrid 3D mesh with a boundary layer zone as shown in Figure 5. The GMSH provides extrude feature for prism layer mesh with gradual size steps to resolve viscous boundary layer over which the unstructured tetrahedral mesh can be created. The height of the wall adjacent cell was calculated for Mach no = 0.7 and Reynolds no = 1.773e6 to be 8e-06 m. Note that the last prism layer cell before the unstructured mesh starts is almost square cross section. GMSH can be used to classify every surface

according to the individual or group of boundary conditions. The mesh refinement using for each edge is also defined for clustering as required. To eliminate the boundary effects on the CFD results, a large flow domain, with 20Dx20D in cross section and 20L in length, is selected.

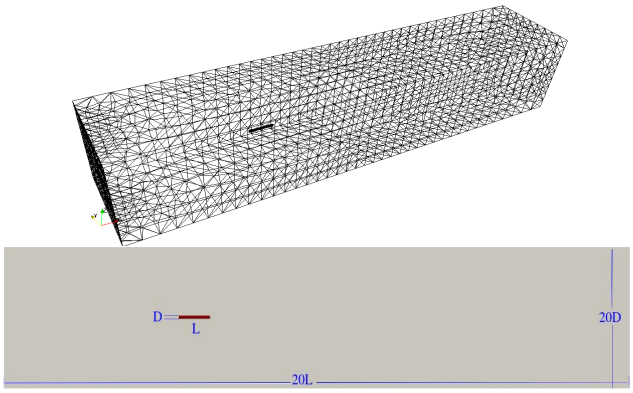

Figure 5: Computational domain is 20x in all directions.

Table 1: Grid sensitivity study at Mach no 0.7 at alpha=4 deg.

Mesh Size	Pressure Recovery	Error %
750000	0.8935	1.380
1550000	0.898	-0.504
2500000	0.899	-0.111
3250000	0.8995	-0.056
6020000	0.8996	-0.011
Ref [7] Sun Shu et al	0.906	0

The baseline case was run in SU2 direct flow solver for the following boundary and flow conditions:

- RANS solution for Mach no = 0.7 and Re no = 1.773e6
- Wall surfaces taken at no-slip adiabatic condition
- Intake exit is the AIP with pressure outlet BC of 0.9bars.

In the flow domain the truncation error highly depends on the grid resolutions. Therefore, it is important to choose a grid size that is sufficiently fine to solve the flow domain accurately for this specific problem and that is small enough to save computational time. To determine the grid sensitivity involved in the numerical study of the submerged inlets, a sequence of five grids with increasing resolution is used as shown in Table 1. The reference value is 0.906 and for an error of -0.504 % the size of the mesh obtained from mesh optimization study was 1.55 million cells. Solutions are performed on the parallel computer system which is in the HPC lab of METU Center for Wind Energy (RÜZGEM). The cluster consists of 8 nodes with 4 AMD® Opteron™ 6276 CPUs (16 cores, clocked at 2.30 GHz) per node, totaling up to 512 cores [13].

The convergence time of each CFD solution and adjoint is 2 hours each approximately while an additional 2-2.5 hours are required for each design for mesh deformation depending upon the degree of deformation . Therefore for a 100 design cycle optimization 280 hours are approximately required.

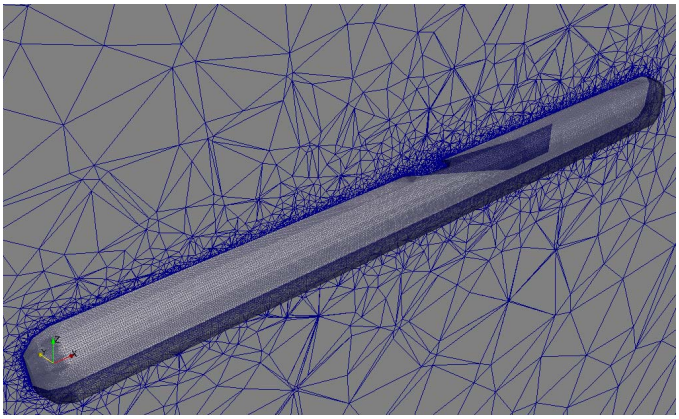

a. Mesh on body surface and center plane

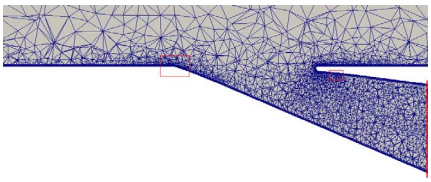

b. Close up view of center plane section mesh around intake

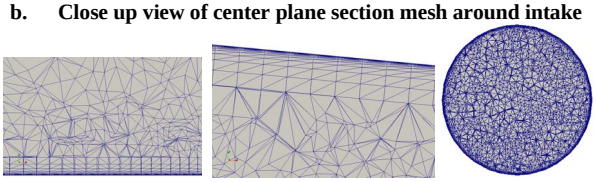

c. Mesh at different locations of intake.
Left : Onset of ramp, Centre:q Aft of the rear lip Right: AIP section

Figure 6: 3D hybrid mesh using GMSH

B. Fluid flow and Optimization equations

Adjoint equation for shape optimzation using different functionals were implemented into SU2 suite by Kline [10]. A brief review of the governing equations are presented . The governing flow equations are given as:

$$\frac{\partial \rho}{\partial t} + \vec{\nabla} \cdot (\rho \vec{u}) = 0$$

$$\frac{\partial (\rho \vec{u})}{\partial t} + \vec{\nabla} \cdot [\overline{\rho u \otimes u}] = -\vec{\nabla} p + \vec{\nabla} \cdot \bar{\bar{\tau}} + \rho \vec{f}$$

$$\frac{\partial (\rho e)}{\partial t} + \vec{\nabla} \cdot ((\rho e + p)\vec{u}) = \vec{\nabla} \cdot (\bar{\bar{\tau}} \cdot \vec{u}) + \rho \vec{f} \vec{u} + \vec{\nabla} \cdot (\vec{q}) + r$$

Given that the flux vector U:

$$U = \begin{Bmatrix} \rho \\ \rho \vec{u} \\ \rho e \end{Bmatrix}$$

SU2 can solve PDEs that are governing a physical system of a fluid mechanics problem and are written the following expression:

$$\frac{dU}{dt} + \nabla.F^c - \nabla.\mu F^{\nu k} = Q$$

The convective and viscous fluxes and heat transfer and source terms are:

$$F^c = \begin{bmatrix} \rho\nu \\ \rho\nu\nu + \bar{\bar{I}}p \\ \rho E\nu + p\nu \end{bmatrix}; F^{\nu 1} = \begin{bmatrix} - \\ \bar{\bar{\tau}} \\ \bar{\bar{\tau}}.\nu \end{bmatrix}; F^{\nu 2} = \begin{bmatrix} - \\ - \\ C_p \nabla T \end{bmatrix}; Q = \begin{bmatrix} q_\rho \\ q_{\rho\nu} \\ q_{\rho E} \end{bmatrix}$$

The governing equation is now reorganized to define the residual,

$$R(U, X) = \frac{dU}{dt} + \nabla.F^c - \nabla.\mu F^{\nu k} - Q = 0$$

The gradient of which is the function of the residual that will converge to zero and provide the necessary constraint equations.

$$\frac{dR}{d\theta} = \frac{\partial J}{\partial U}\frac{dU}{d\theta} + \frac{\partial J}{\partial X}\frac{dX}{d\theta} = 0$$

The formulation of adjoint based aerodynamic optimization is discussed in several studies and recently started to be implemented in different computational platforms. A form of governing equation can be written in the following semi-discrete form:

$$R(U, X) = 0.$$

Here X is the mesh coordinates.

The objective function J depends on the mesh points and flow variables which depend upon, the space coordinates,

$$J(U, X(\theta))$$

differentiating with respect to design variable gives another differential equation in which we can define our multiplier functions.

$$\frac{dJ}{d\theta} = \frac{\partial J}{\partial U}\frac{dU}{d\theta} + \frac{\partial J}{\partial X}\frac{dX}{d\theta}$$

After some rearrangement and manipulations, the details of which can be found in ref [5] we obtain the adjoint equation:

$$\left(\frac{\partial J}{\partial U} + \Psi^T \frac{\partial R}{\partial U}\right) = 0$$

Where Ψ^T is the adjoint. The remaining part of the gradient of the objective function is written as:

$$\frac{dJ}{d\theta} = \frac{\partial J}{\partial X}\frac{dX}{d\theta} + \Psi^T \frac{\partial R}{\partial X}\frac{dX}{d\theta}$$

$$\frac{dJ}{dX} = \frac{\partial J}{\partial X} + \Psi^T \frac{\partial R}{\partial X}$$

The gradient with respect to mesh coordinates will finally give the surface sensitivity:

$$\phi = \frac{dJ}{dX_S} = \frac{dJ}{dX}\frac{dX}{dX_S}$$

Hence objective function sensitivity is function of volumeetric sensitivity and shape parameterization function. The surface is parameterized using FFD control point method in the present study.

C. FFD Box for Shape Parameterization

Shape optimzation mathematically resolves complex geometrical surfaces in order to give control while deforming with respect to the given sensitivity of objective function. For 3D shapes , CAD based and FFD box methods are generally empoyed [11]. In the present study, in order to shape parameterize the design variable surfaces, FFD box method is utilized which can be implemented by the SU2 DEF tool.

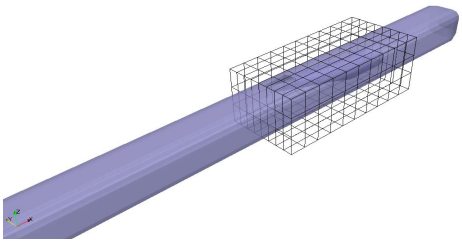

Figure 7: FFD Box enclosing the intake which is the design variable

FFD box method uses point inversion by which cartesian based surface points relate to parametric lattice points which control the shape deformation [12]. By employing point displacement and smoothening iterations generate a new surface over the baseline geometry. The volume mesh is then adjusted for the new surface by using spring analogy.

The settings in the script require the definition of the design variable in which the only the intake portion of the surface is under consideration while the rest of the flat plate is constrained and will not act as part of the design variable as shown in figure 7. The control point configuration for the present case is (8,8,11). The FFD box method requires point inversion technique in which the control points on the well-defined box, which encloses the surface, can control the deformation of the mesh points on the surface by spring-deformation analogy while 2nd order shape deformation solver is used.

III. Flow Solutions

The turbulent flow solutions are obtained on a baseline grid as well as the solution adapted grid. SST model are used to resolve the flow. The results are presented for the multi-objective optimization of a submerged intake on 3D slender aerodynamic body at Mach no 0.73 and angle of attack 0 degree. The flow is solved for the complete body with local shock at the nose and wake formation at the body base as shown in figure 8. However, the region of interest in the present study is the flow in and around the trapezoidal submerged intake.

A. *Baseline Solutions*

Initially, the baseline geometry is discretized using GMSH and direct solution on the mesh is obtained using SU2 CFD. The streamlines over the complete body are shown in figure 8.

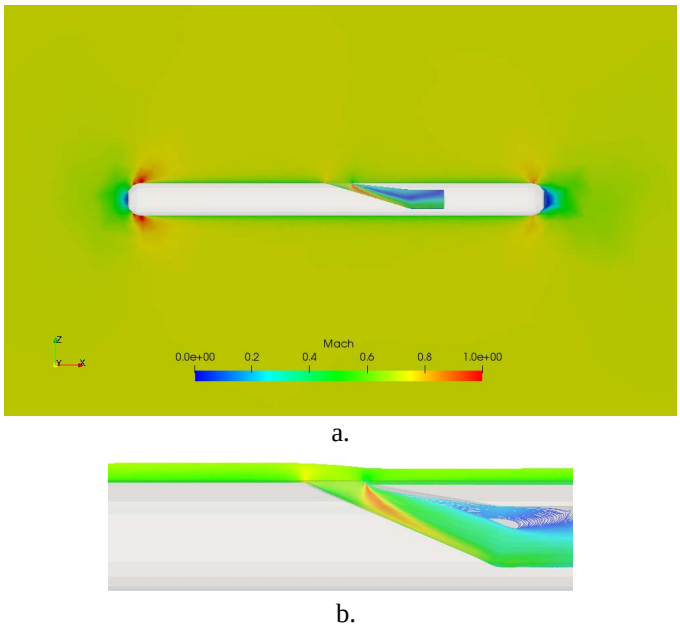

Figure 8: Flow illustration showing Mach distribution on centre plane
a. Mach filled contours b. Streamlines around intake

Streamlines for both along surface plane and across center plane are shown. It can be observed that flow enters the intake smoothly and remains attached along the ramp however separation occurs aft of rear lip on the duct upper surface. The separation is accompanied by shock formation and counter rotating vortex pair in the re-circulation zone. This flow causes pressure losses but at the same time increase pressure distribution over the duct upper surface and thus create the pressure differential to give lift. The flow is further illustrated in the region of interest using captured streamline visualization in Figure 9.

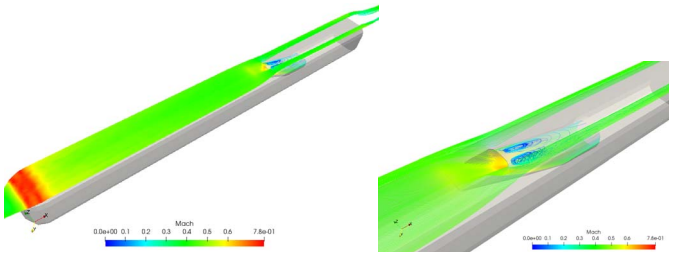

Figure 9: Intake captured streamlines illustrating flow in and around intake

Intuitively, for a clean body with no intake, lift does not exist at zero angle of attack. In the present study, the aim is to improve the intake performance at the duct AIP as well as obtain certain positive lift. Therefore, the optimization of intake duct requires a combined objective function in the optimal shape design definition with weighted individual pressure and lift functions as mentioned in previous section. The results of the present CFD study on the baseline geometry are already compared for grid sensitivity study in Table 1. The compared pressure outlet results are in good agreement with reference results [2].

B. *Adjoint Calculation*

Aerodynamic shape optimization technique relies upon calculation of sensitivity of the design variable. In order to have automatic shape optimization as shown previously in the flow chart, adjoint or sensitivity calculation is done using shape parameterization which is FFD control point method in this study. The FFD box information is embedded in the SU2 file after the mesh is generated. The direct CFD solution obtained from the baseline are employed to find the sensitivity of objective function due to the deformation of the design variable with respect to the given control point movement on FFD box using the equations derived. The multi-objective optimization presented in the study requires definition of weights for each design objective, that is , CL/CD and pressure at AIP, inside the main script to give a combined or multi-objective function.

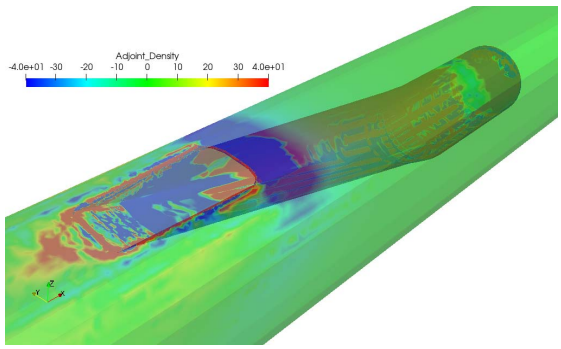

Figure 10: Adjoint for combined objective function

C. *Shape Optimization*

The design iterations are done after the calculation of adjoint- in which the control points defined in FFD box deform the design variable surfaces within given movement limits.
The design optimization cycle with 100 iterations of shape deformation and direct solutions finally resulted in the optimized shape. At the end of the optimization iterations, the total pressure at AIP increases from 1.055 bars to 1.067 bars which corresponds to reduction in loss of 10% keeping the mass flow rate in the range of 0.224 to 0.226 kg/s.

The results for baseline geometry give negative lift however after the optimization cycles, CL/CD increases from -0.075 to +0.016 as shown in figure 12. The shape optimization for the objective functions was possible due to the deformation in shape of the design variable which were defined as the intake surfaces while the body surfaces remained intact. The centre plane view of the intake section is shown in figure 13. There is a prominent variation in the rear lip shape which increases in

thickness as well as sharp corner at the edge is replaced by a smooth curvature. The less prominent variation is in the ramp aft the fore lip where a depression is observed compared to the baseline. In the section view of the intake the edges are observed to get smooth and corners are replaced by curves as seen in figure 13 due to the design optimization procedure.

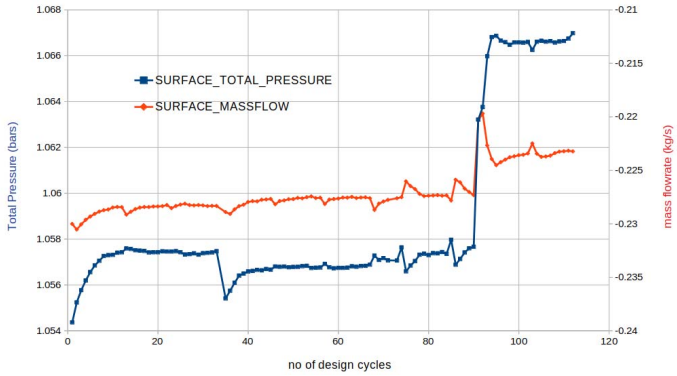

Figure 12: Pressure outlet at AIP for Optimzation cycles.

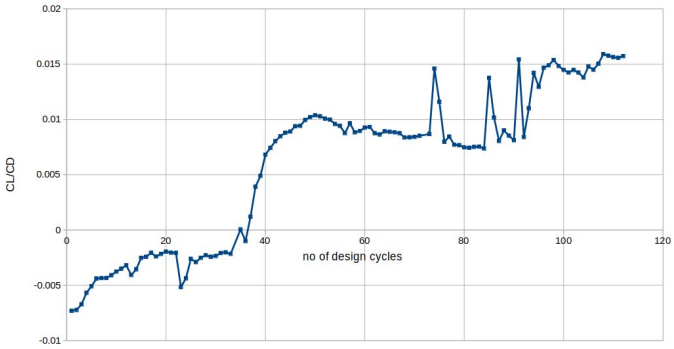

Figure 12: CL/CD for Optimzation cycles.

The duct cross section is observed to have deformed as well in the mid-section view as shown in figure 14.

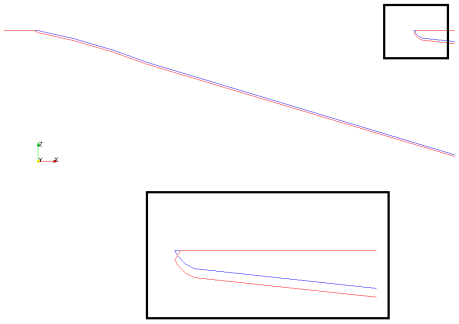

Figure 13: Outline of intake section at centre plane

Blue: Baseline; Red: Final Design

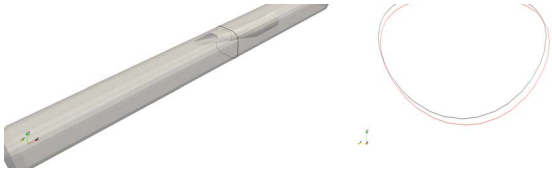

Figure 14: Outline of intake section at duct centre.

Blue: Baseline; Red: Final Design

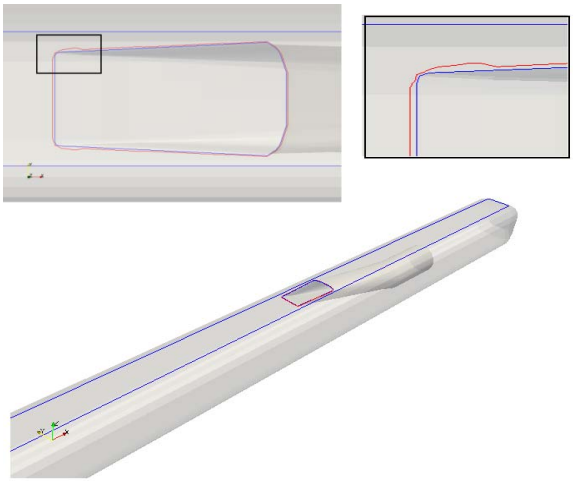

Figure 15: Outline of intake section from top view.

Blue: Baseline; Red: Final Design

The top view of the intake as placed in the body as shown in figure 15 illustrates the outlines of both baseline and optimized design as blue and red, respectively. The change in the shape of the corners near the fore lip and onset of the intake ramp is vividly observable. Ultimately the main interest of the design cycle which is to transform the baseline flow into an optimized one is seen in following paragraphs. The shape deformations as visualized using detained overlapping outlines of sections at different locations of the intake. The strong flow separation due to sharp rear lip is now replaced by a milder separation which improves the overall pressure distribution as illustrated in figure 16.

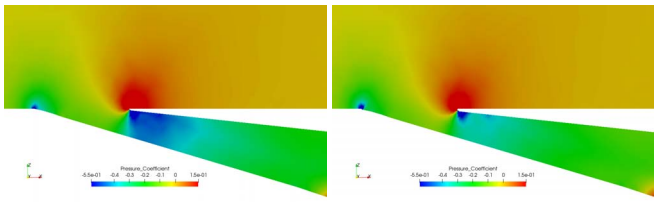

Figure 16: Pressure distribution for intake at centre plane.

Left: Baseline; Right: Final Design

The static pressure on the duct section just upstream of the AIP is shown in figure 17 indicating improved distribution due

to the optimization process. The separation in flow causes losses in pressure recovery but at the same time create the differential in duct surface Cp distribution which creates the lift. Note that the baseline shape gives negative value of lift but after shape deformation positive lift is consequently obtained. It should be noted here that the presented outlines of the baseline and deformed shapes are on scale and not exaggerated for visualization purposes.

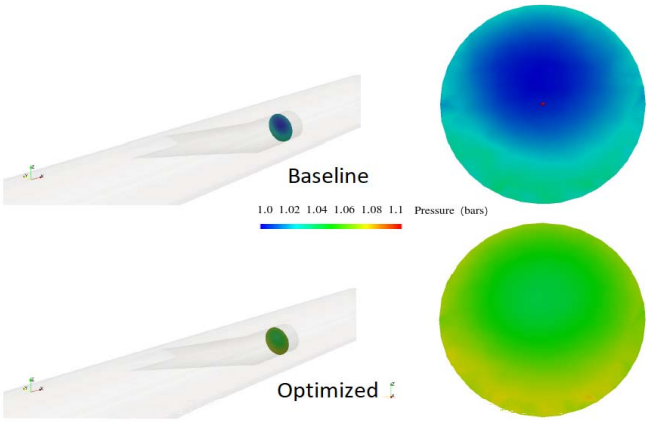

Figure 17: Pressure at AIP section.

Top: Baseline; Bottom: Final Design .

D. Cp Distribution variation along different intake surfaces

In order to understand the effect of shape deformation on the lifting effect created by the intake, the Cp distribution at different regions inside and outside the intake were analyzed. The Cp along the center line of intake ramp is shown in figure 18. This region of the intake is exposed to the top view of the body. The graph indicates a decrease in Cp from baseline to optimized value.

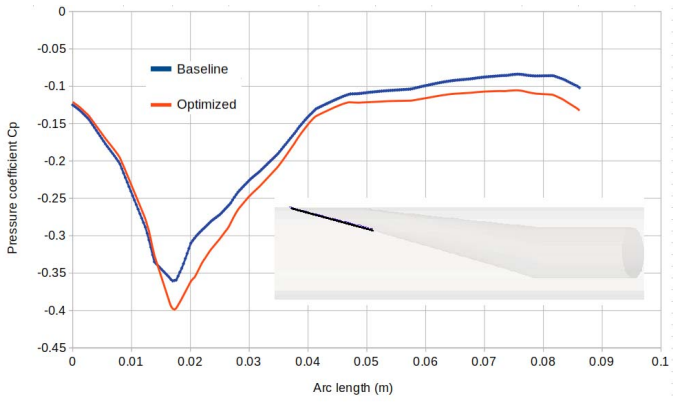

Figure 18: Cp distribution along ramp

The connecting duct is considered as the inner surface aft the ramp where the Cp distribution is meaningful in terms of differential between upper and lower surfaces of the duct. The ΔCp distribution at the duct center lines are illustrated in figure 19 and 20 for the slant and straight portions separately.

In both cases the optimized shape shows a reduction in differential pressure and indicate a greater contribution to lift.

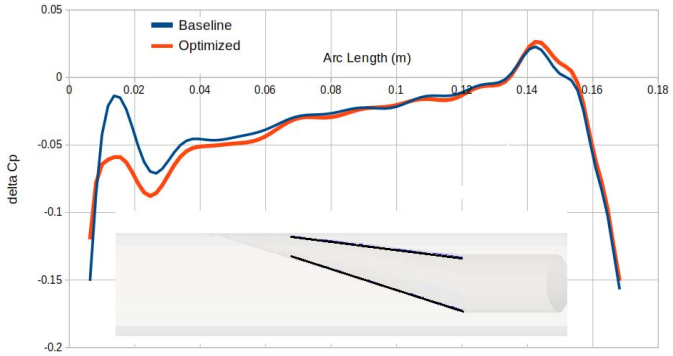

Figure 19: ΔCp distribution on connecting duct

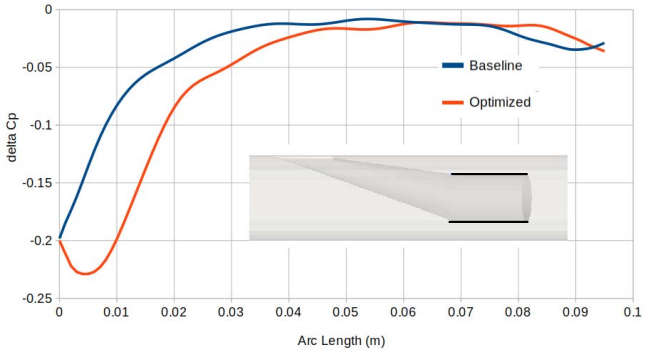

Figure 20: ΔCp distribution on inner constant area duct

The Cp distribution on the region on the body surface downstream of the intake is shown in figure 21. The pressure coefficient is positive at the edge and gradually subsides to become almost negligible at 0.1 m distance. This region is generating a force opposite to the lift direction however due to the optimization process there is a slight decrease in maximum Cp value which helps in improvement of overall lift.

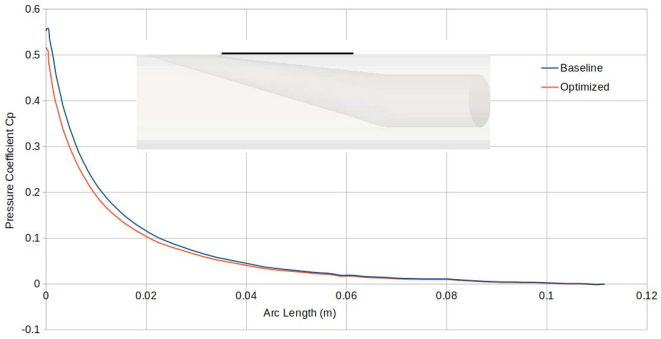

Figure 21: Cp distribution on body aft intake rear lip.

IV. CONCLUSIONS

In the present study the trapezoidal submerged intake on a slender aerodynamic body was studied for multi-objective optimization using adjoint based techniques and FFD box by employing SU2 platform suite. The objective functions, lift and total pressure were combined with drag as the constraint which was included into the combined objectives as the penalty function. The objective functions were all assigned different weights. The results at the end of optimization cycles increases the CL/CD from -0.075 to +0.016 the total pressure at AIP increases from 1.055 bars to 1.067 bars which corresponds to reduction in loss of 10% keeping the mass flow rate in the range of 0.224 to 0.226 kg/s.

The study demonstrated the use of different tools for aerodynamic shape optimization. The use of combined objective function was necessary due to the counterproductive nature of the individual objective functions and therefore any future optimization study on such submerged intakes can be done by considering different combinations and weighted scales of individual objective functions. While the pressure recovery at AIP remains the primary objective however lift can also be included in a trade-off between submerged intake and pitot type as an added advantage.

REFERENCES

[1] Emmet A. Mossman, Lauros M. Randall, *An Experimental Investigation of the Design Variables for NACA Submerged Duct Entrances*, NACA MEMORANDUM, Published on Jan 8, 1948.

[2] J.SEDDON, E.GOLDSMITH: "*Intake Aerodynamics*", AIAA Education Series, 1985.

[3] Csar Celis Perez, and Sandro Barros Ferreira, and Lus Fernando Figueira da Silva, J *Computational Study of Submerged Air Inlet Performance Improvement Using Vortex Generators*, JOURNAL OF AIRCRAFT Vol. 44, No. 5, September October, 2007.

[4] *Jameson*, A., Pierce, N.A. and Martinelli, L., *Optimum aerodynamic design using the Navier-Stokes equations*. AIAA Paper 97–0101 1997.

[5] Brezillon, J. and Gauger, N. R., "*2D and 3D aerodynamic shape optimization using the adjoint approach*," Aerospace Science and Technology, Vol. 8, 2004, pp. 715–727.

[6] EZGI S. TASKINOGLU, *A MULTIOBJECTIVE SHAPE OPTIMIZATION STUDY OF A SUBSONIC SUBMERGED INLET*, Phd Thesis Rutgers The State University of New Jersey May , 2004.

[7] Shu Sun, Rong-wei Guo, Yi-Zhao Wu, *Characterization and Performance Enhancement of Submerged Inlet with Flush-Mounted Planar Side Entrance* Journal of Propulsion and Power *23(5):987-995 September* 2007 .

[8] Thomas D. Economon, Francisco Palacios, Sean R. Copeland, W. Lukaczyk, and Juan J. Alonso *SU2: An Open-Source Suite for Multi physics Simulation and Design.* AIAA Journal Vol. 54, No. 3, March 2016.

[9] Geuzaine, C. and Remacle, J. F., "GMSH: a three dimensional finite element mesh generator with built-in pre- and post-processing facilities," International Journal of Numerical methods in Engineering, Vol. 79, 2009, pp. 1309–1331.

[10] Kline, H.L., "*The continuous adjoint method for multi-fidelity hypersonic inlet design*", PhD thesis, Department of Aeronautics and Astronautics, Stanford University 2017.

[11] Agarwal, Dheeraj and Marques, Simão and Robinson, Trevor and Armstrong, Cecil and Hewitt, Philip. *Aerodynamic Shape Optimization Using Feature based CAD Systems and Adjoint Methods.* Conference: 18th AIAA/ISSMO Multidisciplinary Analysis and Optimization Conference Denver, Colorado , 2017.

[12] Samareh, J. A., "*Survey of shape parameterization techniques for high-fidelity multidisciplinary shape optimization*," AIAA journal, Vol. 39, No. 5, 2001, pp. 877–884.

[13] Önel, Hüseyin & Tuncer, Ismail, *A comparative study of wake interactions between wind-aligned and yawed wind turbines using LES and actuator line models.* Journal of Physics Conference 2020.